Verification and Validation of *hyFoam* for Supersonic External Flows

Jimmy-John O.E. Hoste[*], Vincent Casseau[†]

May 23, 2021

Abstract

This technical report is intended as supplementary material to the test cases associated with the *hyFoam*[1] open-source CFD solver, part of the larger *hyStrath* platform [2]. It provides a detailed description of validation geometries that are commonly tested during the development of supersonic/hypersonic CFD solvers and which are relevant to cold flow conditions.

1 Introduction

The *hyStrath* open-source CFD platform has been initiated in 2014 with the creation of the *hy2Foam* solver [1, 2] to tackle hypersonic flows in thermal nonequilibrium conditions that are typical of atmospheric re-entry conditions. During its development, a derived solver, *hyFoam*, has been added with the intent to address high-speed flows in thermal equilibrium conditions that can for instance be found in scramjet flow paths [3]. Scramjet simulations would not be made possible without the consideration of simplified test cases presenting some of the physical aspects encountered in such flows. These studies have been performed in 2014-2016 and are now provided to assist *hyFoam* users.

As an aid to the verification step, another open-source CFD solver is considered to allow code-to-code comparison: Eilmer. Developed at the University of Queensland with its origins dating back 1991, it was intended to provide similar capabilities to the SPARK code [4, 5, 6] but with new computational technology. The solver has been complemented with many additional features in recent years, making it adequate to compute scramjet type flows. At the time of this study, the Eilmer CFD package's stable release was called Eilmer3 and it was thus used to obtain the results presented herein. Please note that a new

---

[*]Currently: Postdoctoral Researcher at CERFACS, France.
[†]Currently: Postdoctoral Researcher at McGill University, Canada
[1]https://vincentcasseau.github.io/solvers-hyfoam/
[2]https://vincentcasseau.github.io/

project named Eilmer4[3] [7, 8] started in June 2015.

The following sections present the results of the comparative study between the *hyFoam* and Eilmer3 solvers, aiming at evaluating their respective capabilities in handling canonical high-speed flow fields. A laminar flat plate is first selected in Section 2, and is then followed by a ballistic flare in Section 3 and finally a turbulent flat plate in Section 4.

To cite this technical report, please do so as follows:

@TechReport{hostecasseau2021_TR-HS-1.1,
Title = {Verification and Validation of hyFoam for Supersonic External Flows},
Author = {Hoste, J-J. O.E. and Casseau, V.},
Year = {2021},
Month = {May},
Institution = {hyStrath TR-HS-1.1},
Note = {Available at `https://github.com/vincentcasseau/hyStrath/`}

---

2 The Laminar Flat Plate

A pivotal test case for evaluating the high-speed capabilities of a CFD solver is that of a laminar flat plate. The boundary layer has been investigated both numerically and experimentally, *e.g.*, by Bernman, Anderson and Drummond [9], who used a two-dimensional laminar flat plate as a first validation test case for their code. The same test case has been simulated by Espinoza *et al.* [10] with OpenFOAM's *rhoCentralFoam* solver. Both studies are retained and their data will be compared to the predictions of *hyFoam* and Eilmer3.

2.1 Problem formulation

Figure 1 shows the two-dimensional computational domain used in the simulations. The plate, marked in red, has a length L of 0.1 m and the domain extends 0.02 m upstream its leading edge (LE). The flow conditions reported in [10] are selected. The working fluid is standard air, modelled as an ideal gas, with a ratio of specific heats (γ) of 1.4. A freestream inlet temperature, T_∞, of 300 K is prescribed as well as a Mach number (M) of 2 and a Reynolds number, Re_∞, of 500[4] Freestream pressure and velocity are consequently set to $p_\infty = 114.46$ Pa and $u_\infty = 694.55$ m/s respectively. The ratio of the flat plate

---

[3]`http://cfcfd.mechmining.uq.edu.au/docs/tools/eilmer/`
[4]The reference length is taken equal to 0.01 m.

temperature to the freestream temperature, T_w/T_∞, is equal to 2 and no slip conditions are assumed. A slip wall boundary condition (BC) is selected for the part of the domain preceding the flat plate. Sutherland's law is employed for the calculation of the species viscosity and thermal conductivity. The initial solution is set using inflow conditions and simulations are performed with the Euler explicit time scheme and a Courant-Friedrichs-Levy (CFL) number of 0.5.
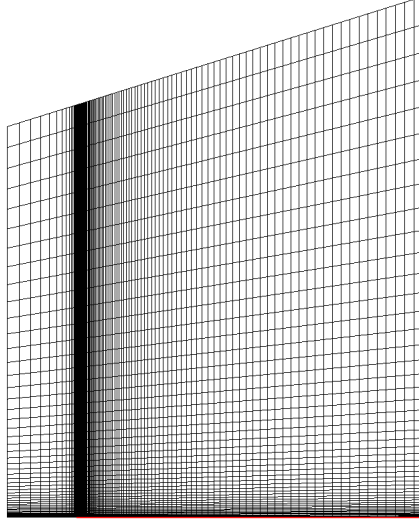

Figure 1: Computational domain for Anderson's laminar flat plate simulations with the plate marked in red.

2.2 Grid independence

A mesh independence study has been performed in Eilmer3 and makes use of the grid convergence index (GCI) introduced by Roache [11]. The method uses three different grids with a refinement factor of at least 1.1 to differentiate the discretization error from other sources of error. An estimate of the quantity of interest for an infinitely fine grid is provided through Richardson's extrapolation. More details about the rationale and computations may be found in the elaboration of Slater [12] or in the work of Roache [11]. It must be noted that this method's evaluation criterion is only concerned by the spatial convergence and that the refinement is global.

Three meshes are considered with a global grid refinement ratio of 2 as shown in Table 1. N_x and N_y are the number of cells in the horizontal and vertical directions, respectively. The parameter of interest for this study is the local

skin friction coefficient, C_f, as it is highly sensitive to the grid size. Its value at a position located 0.01 m downstream the leading edge of the flat plate is monitored and graphed. The skin friction is computed according to the formula given in Equation 1, which uses the dynamic pressure at the boundary layer edge (here denoted by an index "e"). This is common practice in studies of compressible boundary layers of flat plates as the freestream conditions differ in general from the flow conditions close to the edge of boundary layer due to the presence of shocks.

$$C_f = \frac{\tau_w}{0.5\rho_e u_e^2} \tag{1}$$

Grid no	Qualifier	N_x x N_y
1	fine	460 x 400
2	medium	230 x 200
3	coarse	115 x 100

Table 1: Grids considered for the GCI computations for the laminar flat plate.

The results of the mesh independence study are given in Figure 2. The horizontal axis is a normalized grid spacing obtained by dividing the total number of cells of each mesh by the total number of cells of the finest mesh. Consequently, the C_f prediction at a normalized grid spacing of 1 is the value obtained with the finest mesh. Richardson's extrapolated value for C_f equals 0.0326225 and the coarse and medium grids are shown to be within an error band of 0.4 % and 0.1 % of that value, respectively. The GCI values of the grids presented in Table 1 thus ensure predictions within the asymptotic range of convergence and the coarse grid results are deemed reliable enough and considered to be mesh independent.

2.3   Results

Figure 3 presents Bernman *et al.* data[9], labelled as "Anderson" and "Integral solution", Espinoza *et al. rhoCentralFoam* solution [10] and results from both solvers. The x-component of the velocity vector, scaled by the freestream value, at $x = 0.01$ m shows a good concordance between all data sources and a similar observation can be made for the skin friction coefficient in Figure 4.
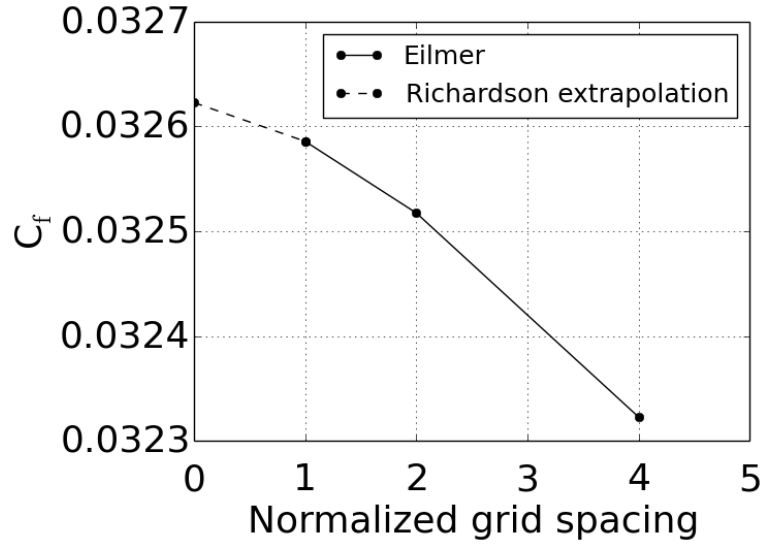
4

Figure 2: C_f predictions for the flat plate are within the asymptotic range of convergence.
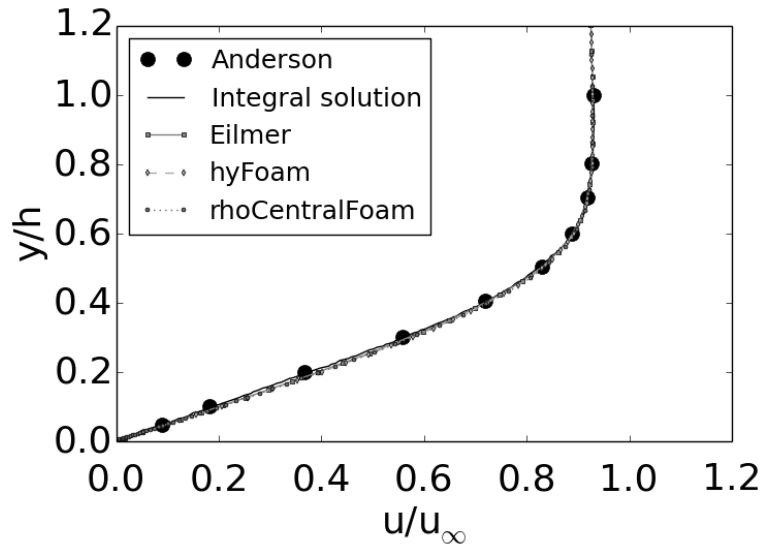

Figure 3: Velocity profile across the boundary layer at $x = 0.01$ m for the laminar flat plate test case.
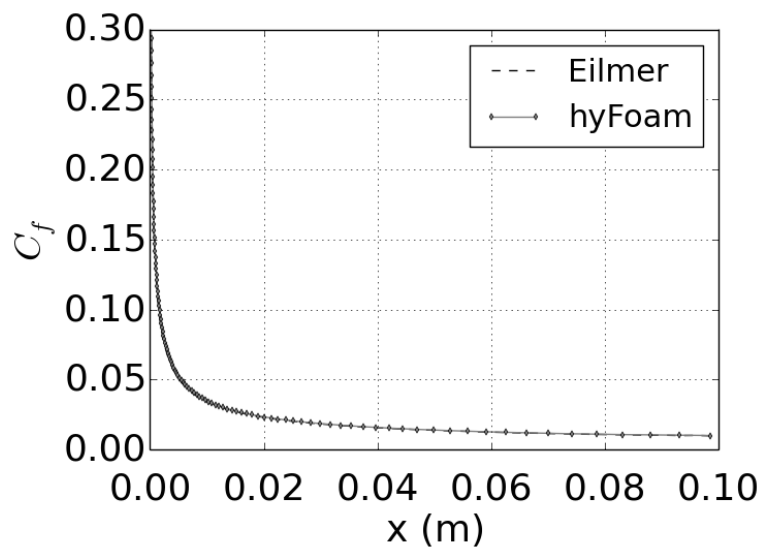
Figure 4: Skin friction coefficient for the laminar flat plate test case.

3 HB-2 Flare

The HB-2 configuration is selected to evaluate the heat flux predictions of both solvers without the effects of turbulence. In the design phase of hypersonic vehicles and integrated engines the thermal loads need to be estimated and CFD codes are expected to reliably provide such information.

3.1 Problem formulation and grid selection

The HB-2 standard hypersonic ballistic configuration model sketched in Figure 5 has been studied experimentally by the Japanese Aerospace Exploration Agency (JAXA) [13, 14] in their hypersonic wind tunnel at stagnation enthalpy conditions of 1 MJ/kg. The air mixture is treated as a calorically perfect gas and the supersonic inflow conditions retained in this work, listed in Table 2, coincide with the 2.5 MPa reservoir total pressure conditions in [13].
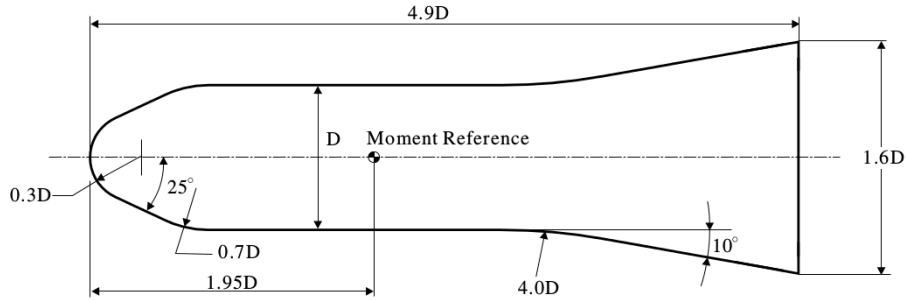

Figure 5: Geometry of the HB-2 flare as presented in [13].

Variable	Units	Value
M_∞	-	9.59
p_∞	Pa	75.0
T_∞	K	52.0
ρ_∞	kg/m^3	5.0×10^{-3}
Re_∞	1/m	2.1×10^6

Table 2: Inflow conditions for the HB-2 flare test case.

The geometry in Figure 5 is modelled as a 2-D axisymmetric wedge and the body is treated as a no-slip isothermal wall set at a temperature of 298 K. The grid consists of 141,100 cells, which comes close to Wuilbercq's mesh that totals 137,700 cells [15]. In his simulations that employs the *rhoFoam* CFD solver, grid independence was demonstrated for this mesh size. This is verified in Figure 6

7

where the heat flux profile given Eilmer3 is plotted for two mesh sizes: 35,275 cells for "mesh 1" and 141,100 cells for "mesh 2". It is shown that the variations in heat flux are very small, thus demonstrating grid-independent results. The subsequent comparison with *hyFoam* is performed using "mesh 2".
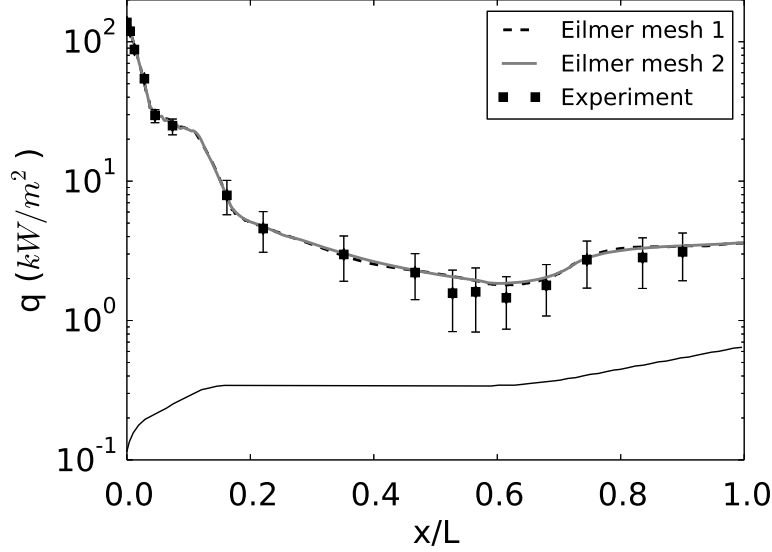

Figure 6: Mesh independence is demonstrated for the HB-2 flare.

3.2   Results

Figure 7 presents the heat flux profile along the geometry obtained by *hyFoam* and Eilmer3 and comparison is made to the experimental measurements. In addition, CFD predictions given by Wuilberq's *rhoFoam* code [15] and Tissera's 5th order WENO solver [16] are graphed as well. The predictions of Tissera's solver appear to capture more heat flux variations along the geometry. Nevertheless, all other solvers fall within the range of experimental uncertainty and the Eilmer3 values are very similar to that of *hyFoam*. In conclusion, both solvers are suitable for accurate mechanical and thermal loads computation in supersonic laminar flow conditions.
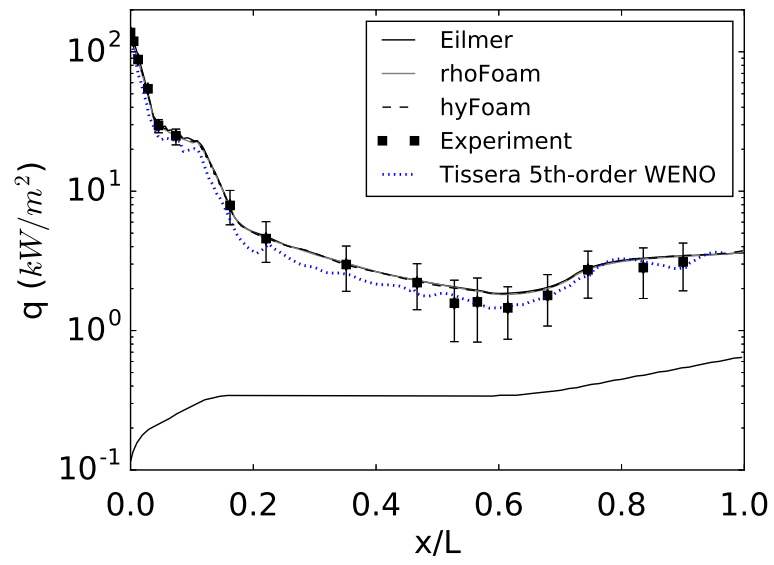
Figure 7: HB-2 flare heat flux predictions of by different solvers.

4   Coles' Turbulent Flat Plate

Scramjet flowpaths are mainly characterized by a turbulent boundary layer, especially in the combustor region. Therefore, a turbulent flat plate is selected to assess the turbulent flow predictions, while validation for non-reacting scramjets can be found in [3].

4.1   Problem formulation

Coles [17] investigated experimentally the boundary layer of a smooth flat plate for up to 80 different test conditions, including valuable information on calibration/instrumentation and data collection. The measurements where performed in a 20-inch supersonic wind tunnel at NASA's Jet Propulsion Laboratory (JPL) and specific attention was drawn to transition and characterization of the turbulent regime. Test case 20 is selected to compare both solvers and is referred to as Coles' experiment in the remainder of this report. It presents a leading edge (LE) fence trip for inducing laminar-turbulent transition of the boundary layer (BL). Data was collected at $x = 21.5$" downstream the LE and local skin friction was measured at two stations ($x = 5.5$" and 13.0"). Freestream conditions were obtained using the ideal gas assumption, isentropic expansion, and Sutherland's law to relate viscosity to the temperature. Experimental conditions tabulated in [17] are summarized in Table 3.

Variable	Units	Value
M	-	3.701
p	cm Hg	103
T	°R	561
x	in	21.48
Re_x	-	3.54×10^6

Table 3: Freestream conditions of test case 20 from Coles' experimental study [17].

The computational domain used in this work is depicted in Figure 8 with the flat plate located at the top of the sketch. An adiabatic wall BC is prescribed for the plate and supersonic inflow conditions are set on the left and bottom domain boundaries. A supersonic outlet is prescribed on the right patch, where values from the interior of the domain are extrapolated. A summary of the CFD supersonic inlet conditions is given in Table 4. Please note that with these freestream values a Reynolds number of 3.66×10^6 is obtained at $x = 21.5$" (or 0.546 m) which results in an error of 3.5 % as compared to the value given in Table 3. Following a sensitivity study on Wilcox' 2006 k-ω model performed using Eilmer3 and reported in the code's turbulence model user guide [18], a turbulent intensity, I, of 5 % and a ratio of turbulent to laminar viscosity (μ_t/μ)

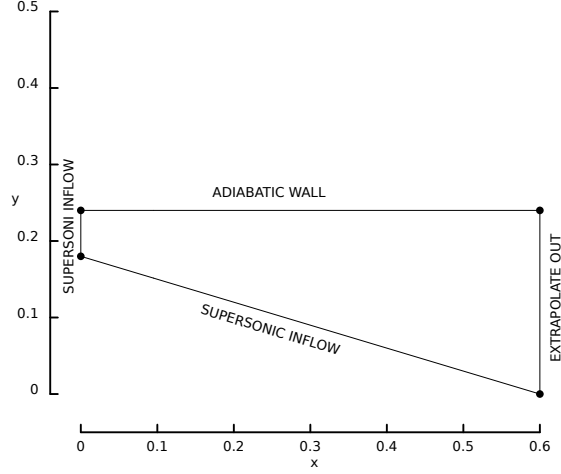of 100 is prescribed. The turbulent Prandtl number, $\mathrm{Pr_t}$, is set to the standard value of 0.9.

Figure 8: Computational domain for Coles' turbulent flat plate.

Variable	Units	Value
M	-	3.701
p	Pa	1358
T	K	83.35
ρ	kg/m^3	0.05675
μ	kg/(m·s)	5.7259×10^{-6}
I	%	5
μ_t/μ	-	100
$\mathrm{Pr_t}$	-	0.9

Table 4: Inlet conditions and turbulent parameters for the CFD simulations reproducing Coles' experiment.

4.2 Grid independence study

The following discussion presents the results of a grid independence study using a GCI based on skin friction in Eilmer3. Table 5 gives an overview of the grid sizes used in the investigation for a cell refinement ratio of 2, with N_x and N_y being the number of cells in the horizontal and vertical directions, respectively, and N_{tot} the total number of cells. All grids ensure a non-dimensional wall distance, y^+, smaller than 1, justifying the choice to not use wall functions.

11

Grid no	Qualifier	N_x x N_y	N_{tot}
1	coarse	50 x 45	2250
2	medium	100 x 90	9000
3	fine	200 x 180	36,000
4	very fine	460 x 360	144,000

Table 5: Grid sizes used in the Coles' flat plate simulations for a total refinement ratio of 2.

The skin friction coefficient at the location $x = 0.546$ m is selected as profiles at this position are later plotted for comparison with experimental data. GCI computations for the coarse, medium and fine meshes doesn't show a grid-independent solution with predictions outside of the asymptotic range of convergence. For this reason a fourth grid has to be generated and the process is repeated with the the medium, fine and very fine grids. This time, the GCI study results in mesh independence of the skin friction predictions as the solutions are within the asymptotic range of convergence. Figure 9 presents the result with a Richardson extrapolated value equal to 0.00159047. The abscissa is the normalized grid spacing previously introduced. It is shown that the "medium" mesh predicts Richardson extrapolated value within an error band of 3.36 %, while C_f for the "fine" mesh falls within an error band of 1.75 % and is therefore retained for further comparisons.
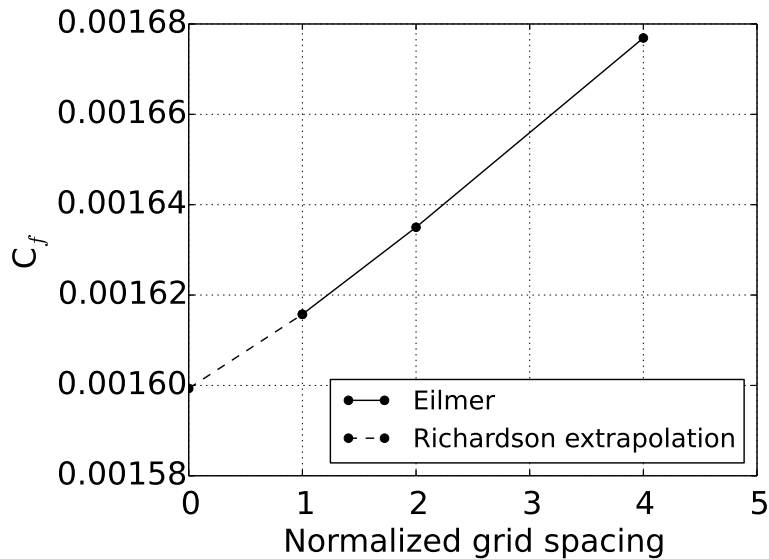

Figure 9: Grid independence study for Coles' experiment.

4.3 Results and discussion

Experimental profiles are taken from an AGARD report on compressible turbulent BL data, that includes Coles' experiment, written by Fernholz and Finley [19]. Data corresponding to the conditions in Tables 3 and 4 are listed under CAT 5301 as 53010801. Not all variables were measured during the experiment and consequently some derivations were used. As known variables, the measured y-position and velocity are introduced with the consideration of a constant total temperature along the profile, *i.e.*, isoenergetic condition. The static pressure is assumed constant throughout the boundary layer and the wall temperature to adiabatic wall (or recovery) temperature ratio ($T_w/T_{ad} = T_w/T_{aw} = T_w/T_r$) is equal to 1. Using Walz's modification [19, 20] of van Driest relation [21] between temperature and velocity, the static temperature is computed as:

$$\frac{T}{T_e} = \frac{T_w}{T_e} + \frac{T_r - T_w}{T_e}\left(\frac{U}{U_e}\right) - r\frac{\gamma - 1}{2}M_e^2\left(\frac{U}{U_e}\right)^2 \tag{2}$$

The recovery factor, r, is defined by the following temperature ratio

$$r = \frac{T_r - T_e}{T_{t_e} - T_e} \tag{3}$$

where the total temperature ($T_0 = T_t$) is obtained through

$$T = \frac{T_0}{1 + \frac{(\gamma - 1)M^2}{2}} \tag{4}$$

The subscript "e" refers to the values at the edge of the BL. In Fernholz's report [19], all data are normalized using this BL edge state. In Coles' experiment it is considered to be the 23rd data point located at y = 0.01556 m. An important remark concerning the experimental data, measured at the location x = 0.546 m, is the uncertainty about the effect of the tripping device (fence trip) used for transiting the boundary layer to a turbulent state. Recreating this effect in CFD is not straightforward and discrepancies are thus expected.

Figure 10 presents the boundary layer profile of the x-velocity component and temperature obtained with Eilmer3 and *hyFoam* for x = 0.546 m. In comparison with experimental data, under-developed CFD profiles are observed and it is attributed to the aforementioned uncertainty associated with the use of a BL trip. The profiles given by both solvers are in good agreement and the small discrepancies near the edge of the boundary layer are most likely a result of the use of different turbulence models and therefore, to their sensitivity to freestream turbulence values.

Figure 11 plots the skin friction coefficient along the plate and its accuracy is assessed using the van Driest II semi-empirical correlation [22, 23] (see Appendix 1 for more details). The shaded area represents the 10 % error band deviation from the van Driest II correlation and both solvers predict a skin friction profile within this error band. Eilmer3's result is closer to van Driest's
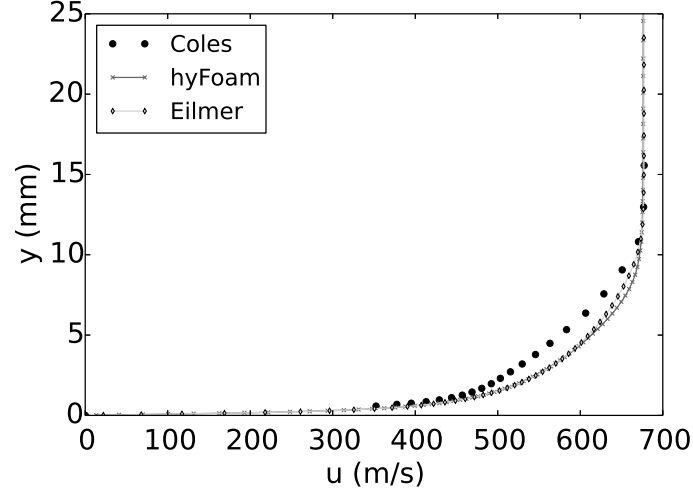
(a) Velocity, x-component
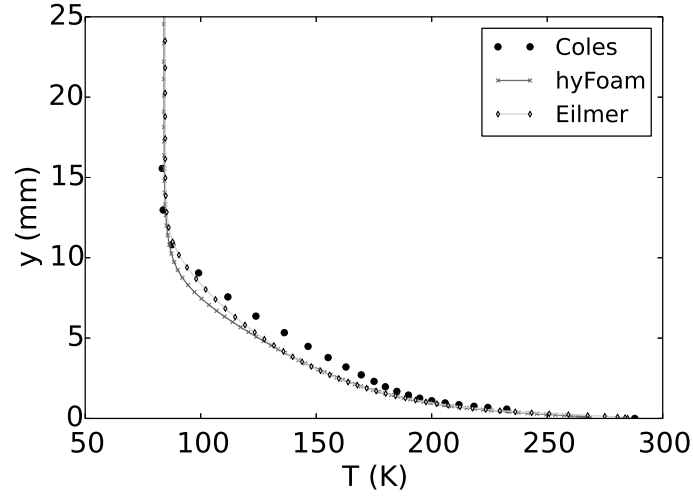
(b) Temperature

Figure 10: Turbulent flat plate predictions at x = 0.546 m.

correlation for most of the plate's length, as compared to *hyFoam*. The CFD predictions differ the most shortly past the LE and they could be caused by different grid requirements and BC in the *hyFoam* solver near the plate's LE. This path has been explored by adding a slip wall upstream the plate but the results

14

however remained unaffected by this change. Considering that the skin friction profiles were superimposed in Section 2 and that they are in close agreement past $x = 0.2$ m in this case, the most plausible explanation becomes the use of two different turbulence models: Wilcox' 2006 k-ω in Eilmer3 and k-ω SST in *hyFoam* – as no common turbulence model existed between the two solvers.

In conclusion, both solvers demonstrate the capability of predicting skin friction within van Driest's error band and can therefore be considered for further simulations.
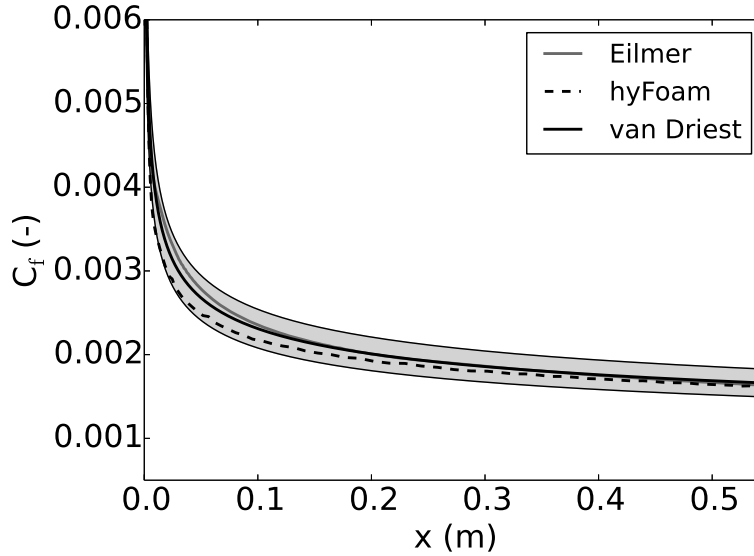

Figure 11: Skin friction coefficient along Coles' turbulent flat plate.

References

[1] V. Casseau, R.C. Palharini, T.J. Scanlon, and R.E. Brown. A two-temperature open-source cfd model for hypersonic reacting flows, part one: Zero-dimensional analysis. *Aerospace*, 3(4):34, 2016.

[2] V. Casseau, D.E.R. Espinoza, T.J. Scanlon, and R.E. Brown. A two-temperature open-source cfd model for hypersonic reacting flows, part two: Multi-dimensional analysis. *Aerospace*, 3(4):45, 2016.

[3] J.-J.O.E. Hoste, V. Casseau, M. Fossati, I.J. Taylor, and R.J. Gollan. Numerical modeling and simulation of supersonic flows in propulsion systems by open-source solvers. In *21st AIAA International Space Planes and Hypersonics Technologies Conference*, page 2411, 2017.

[4] A.D. Cutler, G.S. Diskin, J.P. Drummond, and J.A. White. Supersonic coaxial jet experiment for computational fluid dynamics code validation. *AIAA journal*, 44(3):585–592, 2006.

[5] J.P. Drummond. A two-dimensional numerical simulation of a supersonic, chemically reacting mixing layer. 1988.

[6] M. Carpenter. Three-dimensional computations of cross-flow injection and combustion in a supersonic flow. In *20th Fluid Dynamics, Plasma Dynamics and Lasers Conference*, page 1870, 1989.

[7] P.A. Jacobs and R.J. Gollan. Implementation of a compressible-flow simulation code in the D programming language. In *Applied Mechanics and Materials*, volume 846, pages 54–60. Trans Tech Publ, 2016.

[8] K.A. Damm, R.J. Gollan, and P.A. Jacobs. Verification of the least-squares procedure within an unstructured-grid flow solver. In *20th Australasian Fluid Mechanics Conference*, 2016.

[9] H.A. Berman, J.D. Anderson Jr, and J.P. Drummond. Supersonic flow over a rearward facing step with transverse nonreacting hydrogen injection. *AIAA journal*, 21(12):1707–1713, 1983.

[10] D.E.R. Espinoza, T.J. Scanlon, and R.E. Brown. Validation of tools to accelerate high-speed cfd simulations using OpenFOAM. In *20th AIAA International Space Planes and Hypersonic Systems and Technologies Conference*, page 3566, 2015.

[11] P.J. Roache. *Verification and validation in computational science and engineering*. Hermosa Albuquerque, NM, 1998.

[12] J.W. Slater. Examining spatial (grid) convergence. *Public tutorial on CFD verification and validation, NASA Glenn Research Centre, MS*, 86, 2006.

[13] S. Kuchi-Ishi, S. Watanabe, S. Nagai, S. Tsuda, T. Koyama, N. Hirabayashi, H. Sekine, and K. Hozumi. Comparative force/heat flux measurements between jaxa hypersonic test facilities using standard model hb-2 (part 1: 1.27 m hypersonic wind tunnel results). *JAXA Research and Development Report JAXA-RR-04-035E*, 2005.

[14] S. Kuchi-Ishi, S. Watanabe, S. Ueda, H. Tanno, T. Komuro, K. Sato, and Itoh K. Comparative force/heat flux measurements between jaxa hypersonic test facilities using standard model hb-2 (part 2: High enthalpy shock tunnel results). *JAXA Research and Development Report JAXA-RR-05-030E*, 2006.

[15] R. Wuilbercq. *Multi-disciplinary modelling of future space-access vehicles*. PhD thesis, University of Strathclyde, 2015.

[16] S. Tissera. Assessment of high-resolution methods in hypersonic real-gas flows. 2010.

[17] D. Coles. *Measurements in the boundary layer on smooth flat plate in supersonc flow*. PhD thesis, California Institute of Technology, 1953.

[18] W.Y.K. Chan, P.A. Jacobs, J.P. Nap, D.J. Mee, R.M. Kirchhartz, and Stennett S.J. The k-ω turbulence model in Eilmer3: User guide and test cases. Technical report, The University of Queensland, 2014.

[19] H.H. Fernholz and P.J. Finley. A critical complication of compressible turbulent boundary layer data. Technical report, AGARDograph-AG-223, 1977.

[20] A. Walz. *Strömungs-und Temperaturgrenzschichten*. Braun Karlsruhe, 1966.

[21] E.R. Van Driest. Turbulent boundary layer in compressible fluids. *Journal of the Aeronautical Sciences*, 18(3):145–160, 1951.

[22] E.R. Van Driest. The problem of aerodynamic heating. *Aeronautical Engineering Review*, 15(10):26–41, 1956.

[23] C.J. Roy and F.G. Blottner. Review and assessment of turbulence models for hypersonic flows. *Progress in Aerospace Sciences*, 42(7):469–530, 2006.

[24] D.B. Spalding and S.W. Chi. The drag of a compressible turbulent boundary layer on a smooth flat plate with and without heat transfer. *Journal of Fluid Mechanics*, 18(1):117–143, 1964.

[25] F.M. White. *Viscous fluid flow*. Second Edition, McGraw-Hill New York, 1991.

[26] C.L. Rumsey. Compressibility Considerations for k-ω Turbulence Models in Hypersonic Boundary-Layer Applications. *Journal of Spacecraft and Rockets*, 47(1):11–20, 2010.

[27] W. Mason. *Program FRICTION*. Virginia Tech, Department of Aerospace and Ocean Engineering, Blacksburg, VA24061.

[28] E.J. Hopkins. Charts for predicting turbulent skin friction from the van driest method (II). Technical report, NASA technical note, 1972.

[29] J.R. Carlson. Prediction of very high Reynolds number compressible skin friction. *AIAA Paper-98-2880*, 1998.

[30] R.J. Monaghan. A review and assessment of various formulae for turbulent skin friction in compressible flow. Technical report, Tech. Note No. Aero. 2182, British R.A.E., 1953.

Appendix 1 The van Driest II correlation

Just as with other skin friction correlations, including that of Spalding and Chi [24] and White and Christoph [25], van Driest II uses a transformation to relate the compressible and incompressible forms of C_f, as shown in Equation A1.

$$C_f = \frac{1}{F_c}C_{f,\text{incompressible}} = \frac{1}{F_c}\overline{C}_f \tag{A1}$$

Rumsey [26] presented a comparison of the aforementioned skin friction correlations on adiabatic flate plate cases and demonstrated similar results. The choice of the van Driest II correlation in the present work can thus be justified. Note, however, that when heated walls are considered the approaches result in different estimations with no general certainty on the correctness of each method. In this work the implementation of van Driest II follows the FRICTION program from Virginia Tech [27], which in turn is based on the description of Hopkins [28]. The notation II refers to the theory accounting for the von Kármán mixing length. In the van Driest II method, the transformation function F_c in Equation A1 is given by

$$F_c = \frac{T_{aw}/T_e - 1}{(sin^{-1}A + sin^{-1}B)^2} = \frac{r\frac{\gamma-1}{2}M_e^2}{(sin^{-1}A + sin^{-1}B)^2} \tag{A2}$$

The last equality holds as the adiabatic wall temperature, T_{aw}, is related to the temperature at the edge of the boundary layer T_e as

$$T_{aw} = T_e\left(1 + r\frac{\gamma-1}{2}M_e^2\right) \tag{A3}$$

In both Equations A2 and A3 the variable r represents the recovery factor. A constant value of 0.88 is considered for this parameter to follow the suggestion of Hopkins [28]. Parameters A and B are defined as

$$A = \frac{2a^2 - b}{(b^2 + 4a^2)^{1/2}} \tag{A4}$$

$$B = \frac{b}{(b^2 + 4a^2)^{1/2}} \tag{A5}$$

with a and b given by

$$a = \left(r\frac{\gamma-1}{2}M_e^2\frac{T_e}{T_w}\right)^{1/2} \tag{A6}$$

$$b = \frac{T_{aw}}{T_w} - 1 = \frac{T_e}{T_w}\left(1 + r\frac{\gamma-1}{2}M_e^2\right) - 1 \tag{A7}$$

Obtaining F_c using the method above requires the knowledge of the edge values of Mach number and temperature (M_e and T_e, respectively) as well as the wall

to adiabatic wall temperature ratio (T_w/T_{aw}). The next step consists of determining the incompressible skin friction coefficient, $\overline{C}_f$.

The incompressible skin friction coefficient is found with the use of the Karman-Schoenherr formula for average skin friction (C_F) which yields good results for $Re_x \in [3 \times 10^5, 4.5 \times 10^8]$ [28]. This formula is given in Equation A8 [27, 28, 29].

$$\frac{1}{\sqrt{\overline{C}_F}} = 4.13 \; log_{10}(\overline{C}_F \overline{R}e_x) \tag{A8}$$

where overlined variables denote incompressibility. The length-based Reynolds number is given by

$$\overline{R}e_x = F_x Re_x \tag{A9}$$

with a transfer function defined as

$$F_x = \frac{F_\theta}{F_c} \tag{A10}$$

Equation A10 relates the length-based transfer function (F_x) to the momentum thickness-based transfer function (F_θ). In the van Driest II approach the latter is defined as the ratio of edge to wall viscosity (Equation A11). Please note that the length-based Reynolds number is an input of the program.

$$F_\theta = \frac{\mu_e}{\mu_w} \tag{A11}$$

The viscosity is evaluated with Keyes' formula instead of Sutherland's as it is more accurate for low temperatures below 100 K [23] (it is indeed common to encounter very low freestream static temperatures in hypersonic testing facilities) and both formulas differ by a maximum of 3 percent for temperatures above 111 K [28]. Keyes' viscosity law for air is defined as [23]

$$\mu = a_0 \times 10^{-6} \sqrt{T}/(1 + a_1 T_1/T), \quad T_1 = 10^{-a_2/T} \tag{A12}$$

where the constants a_{0-2} are given by

$$a_0 = 1.488 \quad a_1 = 122.1 \quad a_2 = 5.0 \tag{A13}$$

The Karman-Schoenherr formula is solved in a recursive way using the Newton-Raphson method. For the initial guess the following formula of Blasius [30] is used

$$\overline{C}_F = 0.074 \; \overline{R}e_x^{-1/5} \tag{A14}$$

Once the C_F value is known the local incompressible skin friction coefficient can be obtained with Equation A15, which is the result of differentiating Equation A8 with respect to the length [28].

$$\overline{C}_f = \frac{0.242\overline{C}_F}{0.242 + 0.8686\sqrt{\overline{C}_F}} \tag{A15}$$

Finally, Equation A16 yields the compressible local skin friction coefficient.

$$C_f = \frac{\tau_w}{2\rho_e U_e^2} \tag{A16}$$

It must be noted that Equation A16 is valid when replacing local values by averaged ones. In addition, the momentum thickness-based Reynolds number can readily be obtained as

$$\overline{Re}_\theta = \frac{\overline{C}_F \overline{Re}_x}{2} \tag{A17}$$

and the following equalities hold:

$$\overline{Re}_\theta = F_\theta Re_\theta \tag{A18}$$

$$\overline{Re}_x = F_x Re_x \tag{A19}$$